Indium and phosphorus vacancies and antisites in InP

A. P. Seitsonen, R. Virkkunen, M. J. Puska, and R. M. Nieminen
Laboratory of Physics, Helsinki University of Technology, 02150 Espoo, Finland
(Received 14 April 1993)

We present an extensive study of the structure and energetics of monovacancies and antisites in InP. Using a first-principles approach, the different charge states of indium and phosphorus vacancies and antisites are examined. The lattice distortions around the defects are derived fully self-consistently with respect to both electronic and ionic degrees of freedom. Jahn-Teller relaxations, defect-induced one-electron energy levels, and ionization potentials in the band gap are discussed. From the formation energies we predict the favored vacancies and antisites under different stoichiometry conditions.

I. INTRODUCTION

The characterization of the properties of the III-V compound semiconductors is a subject of growing interest. The emphasis is on the defect-related properties which to a large extent determine the feasibility of the materials for technological use. Although GaAs is the most intensively studied III-V semiconductor, much attention has recently been focused on InP. InP has advantageous characteristics, e.g., for use in many optoelectronic components and in space technology.[1]

Experimentally, vacancies, antisites, and the defects related to them have been observed in InP. Some evidence for the indium vacancy is available from magnetic resonance,[2] photoluminescence,[3,4] and positron-lifetime[5,6] studies of InP. Von Bardelelben[7] has attributed an electron paramagnetic resonance (EPR) spectrum to the neutral phosphorus vacancy in *p*-type InP. Defect complexes including the phosphorus vacancy and zinc impurity have been identified by diffusion studies[8,9] and by positron-lifetime spectroscopy[10] in zinc- and cadmium-doped InP. While indium antisites have not been detected experimentally there are several observations of phosphorus antisite defects in InP. The identification of the *P* antisite was the first successful application of EPR to the study of intrinsic defects in InP.[11] Conventional EPR experiments of the P antisite have been followed by optically detected magnetic resonance methods.[2,12] The analysis of the optically detected electron-nuclear double resonance (ODENDOR) data suggests a tetrahedral geometry of the nearest-neighbor P atoms around the phosphorus antisite in *p*-type InP.[13,14] Very recently, Dreszer *et al.* have assigned the ionization energies of two dominant donor levels in low-temperature molecular-beam-epitaxy-grown InP to the double-donor phosphorus antisite using several experimental techniques. Their results agree with ODENDOR experiments on electron-irradiated InP which determine the $(+/2+)_{P_{In}}$ level position at about 1 eV above the valence-band edge.[16] In *n*-type electron-irradiated samples a metastable defect labelled as the *M* center has been observed by Levinson and co-workers.[17] Based on the theoretical and experimental results of Levinson *et al*, an atomic model is suggested for the *M* center[18] which related the defect to a P antisite-vacancy pair. Also in iron-doped InP, defect complexes exhibit behavior reminiscent of metastability.[19,20] Recently, a metastable defect called the *DX* center has been found in sulfur-doped InP under pressure using optical spectroscopies.[21] The model of the *DX* center in $Al_xG_{1-x}As$ suggests that it is related to a substitutional donor at the cation site accompanied by a large lattice distortion.[22] However, the experimental studies provide mostly indirect information on defects, and the characterization of the defects in a material usually requires information on defects, and the characterization of the defects in a material usually requires extensive comparisons between experiment and theory.

There are a few theoretical studies of the vacancy- and antisite-related defects in InP.[23–29] The ideal P and In vacancies and antisites have been studied using tight-binding,[23–25] density-functional supercell,[26,27] and Green's-function[28] methods. The positions of the ionization levels and the defect states in the band gap have been estimated for the unrelaxed defects.[23–26,28] Jansen[26] has also predicted the formation energies and the relative abundancies of the vacancies and antisites under different stoichiometries. In his calculations the effect of the atomic relaxation has been omitted. The relaxations have been discussed for the neutral anion antisites.[27]

In this work we study the interplay between the electronic states and atomic relaxations of the vacancies and antisites in InP. We use the first-principles Car-Parrinello (CP) scheme[30] to find the ground-state electronic structure and atomic positions with no symmetry restrictions. Previously the method has been applied to various defects in semiconductors, such as vacancies in Si,[31] and vacancies[32] and antisite complexes[33,34] in GaAs. In a recent article we have reported on the negative-*U* effect in the phosphorus vacancy in InP, also calculated within the CP approach.[35] The negative-*U* behavior stems from the strong coupling of the electronic and ionic degrees of freedom that determines the preferred charge state of the defect. In this work we extend the study of InP to a number of different charge states of indium (V_{In}^{2+}, V_{In}^{+}, V_{In}^{0}, V_{In}^{-}, V_{In}^{2-}, and V_{In}^{3-}) and phosphorus (V_P^{+}, V_P^{0}, V_P^{-}, V_P^{2-}, and V_P^{3-}) vacancies, and to indium In_P^{2+}, In_P^{+}, In_P^{-}, and In_P^{2-}) and phosphorus (P_{In}^{2+},

P_{In}^{+}, P_{In}^{0}, In_{In}^{-}, and P_{In}^{2-}) antisites.

In Sec. II we briefly describe the computational method used in the simulations. In Sec. III we discuss the results for the indium and the phosphorus vacancies, and for the indium and phosphorus antisites. The formation energies and the relative abundancies of the defects are also presented in Sec. III. Section IV concludes the results.

II. COMPUTATIONAL CONSIDERATIONS

The Car-Parrinello method is based on density-functional theory (DFT) and the local-density approximation (LDA) for exchange and correlation.[36] The valence-electron density is derived from the electron wave functions, which are expanded in plane waves. The effect of nuclei and core electrons on the valence electrons is treated by pseudopotentials. A detailed description of the method and the relevant equations are presented in e.g., Ref. 37 and are not repeated here.

For indium and phosphorus we use the pseudopotentials of Stumpf, Gonze, and Scheffler,[38] constructed following the scheme of Bachelet, Hamann, and Schlüter.[39] The nonlocal part is treated following the suggestion of Kleinman and Bylander,[40] containing both s and p nonlocal components. s and p electrons are included in the valence. To test the pseudopotential approach we have calculated the ground-state electronic structure of phosphorus clusters with two, six, and eight atoms using both the CP program and an all-electron DFT program.[41] The eigenvalues from the two calculations are in excellent agreement. The energy cutoff of the plane-wave expansion of the electrons is chosen from the convergence of the total energy of bulk InP. We use a cutoff of 15.3 Ry, which corresponds to about 4800 plane waves per eigenstate. The lattice constant of the bulk InP structure is allowed to equilibrate, which ensures that there are no artificial stresses in the system when a defect is introduced. The resulting lattice constant is 5.61 Å, which is 4% smaller than the experimental value of 5.87 Å.[42]

We use a cubic supercell and periodic boundary conditions in all three directions. The cell contains 64 or 63 atoms in the zinc-blende structure. Only one **k** point, Γ, is used to sample the Brillouin zone. The supercell approach with a single **k** point can cause some artificial band structure.[43] However, for ionic III-V compounds, such as InP, the supercell calculations are expected to be more accurate than for covalent semiconductors like Si.[43] For charged defects a rigid background charge density is introduced in order to neutralize the supercell. The defect is introduced at the center of the supercell by removing (vacancy) or by replacing (antisite) one atom in the lattice. The electronic structure of the unrelaxed defect is then optimized using the steepest-descent algorithm.[44] During the dynamics of the ions we use the simulated annealing optimization[30,45] in order to reach the global minimum. However, the steepest-descent method is occasionally needed to bring the electrons back to the Born-Oppenheimer surface. The time step used is 1.3×10^{-16} sec and the electron-mass parameter is chosen as 400 a.u. Good convergence of the total energy is reached typically after ~7000 time steps.

The numerical choices are tested by studying the valence-band structure of bulk InP. In Table I we compare the eigenvalues from our CP simulations to those calculated with an empirical pseudopotential scheme by Cohen and Chelikowski (CC)[46] and with a fully relativistic full-potential linear augmented-plane-wave method (FLAPW),[47] and to the experimental band structure derived from x-ray photoemission spectroscopy.[48] It should be noted that the width of the valence band is decreased in our results if the experimental value for the lattice constant is used. The overall agreement is good, especially with the FLAPW eigenvalues. However, at the maximum of the valence band at the Γ point there is a threefold degeneracy in our results, whereas in the empirical pseudopotential and in the FLAPW calculations the degeneracy has split into two bands. The splitting results from the spin-orbit coupling omitted in our nonrelativistic calculations. The all-electron FLAPW band structure is closest to the experimental values just below the top of the valence band, but the pseudopotential methods give occasionally a better agreement near the bottom of the valence band.

The band gap is underestimated in the FLAPW (and CP) calculations because of LDA[50] and this may cause some difficulties for the deep-level states. In our calculations for the defects all the highest one-electron energy levels of the relaxed defects lie in the experimental band gap. We have checked that the corresponding wave functions of these states are well localized and are therefore not likely to be confused with conduction-band states.

III. RESULTS AND DISCUSSION

A. Indium vacancies

We have studied the electronic and atomic relaxation of the indium vacancies in the charge states from the

TABLE I. The one-electron valence levels in bulk indium phosphide calculated with the Car-Parrinello method (CP), pseudopotential method of Cohen and Chelikowsky (CC, Ref. 46), and fully relativistic full-potential linear augmented-plane-wave method by Massidda *et al.* (FLAPW, Ref. 47), and experimental results (Expt., Ref. 48, except where noted). The zero of the energy scale corresponds to the top of the valence band. All energies are in eV.

k point	Degeneracy	CP	CC	FLAPW	Expt.
Γ_{6v}	1	−11.91	−11.42	−11.60	−11.0
L_{6v}	4	−10.15	−9.67	−9.73	−10.0
X_{1v}	3	−9.39	−8.91	−9.14	−8.9
L_{6v}	4	−6.06	−5.84	−5.90	
X_{6v}	3	−6.01	−6.01	−5.97	−5.9
X_{6v}	3	−2.39	−2.09	−2.46	
X_{7v}	3	−2.39	−2.06	−2.36	−2.2
L_{6v}	4	−0.94	−1.09	−1.11	−1.23
$L_{4,5v}$	4	−0.94	−0.04	−0.98	−1.12
Γ_{7v}	1	0.00	−0.21	−0.12	−0.11
Γ_{8v}	2	0.00	0.00	0.00	0.0
Γ_{6c}			1.50	0.38	1.42[a]

[a]Ref. 49.

doubly positive to the triply negative one. The occupancy of the defect-induced states in the band gap varies from one to six, respectively. In Fig. 1 we show the position and the occupancy of the calculated one-electron energy eigenvalues relative to the top of the maximum of the valence band. The maximum of the valence band is taken from the bulk simulation and the experimental band-gap width is shown in the figure. The dashed lines are the eigenvalues for the unrelaxed vacancies and the solid lines for the fully relaxed configurations. For the indium vacancies the deep levels are all below midgap, and as the number of electrons increases the position of the state rises due to the increased Coulomb repulsion. The positions of the deep levels for the unrelaxed defects are in very good agreement with the semiempirical tight-binding results for undistorted In vacancies in different charge states.[23] Relaxation lowers the energy eigenvalues systematically but does not change the qualitative picture obtained from the unrelaxed vacancies.

Figure 2 shows schematically the distortion of the lattice around the In vacancy in the different charge states. The In vacancy is at the center and the four nearest-neighbor P atoms (filled circles) are at the corners of the distorted cube. Table II lists the amplitudes of the nearest-neighbor relaxations. The breathing mode is the symmetry-conserving relaxation toward (or from) the center of the vacancy, and the pairing modes describe the deviation from the purely radial relaxation. The pairing mode 1 describes the distortion of the nearest neighbors toward (or from) each other within two pairs, and pairing mode 2 is perpendicular to the breathing and pairing-1 components. The negative (positive) sign denotes inward (outward) relaxation in the breathing component and antipairing (pairing) in the pairing-1 component. The amplitudes are given in percent of the bond distance in bulk InP.

According to Table II the breathing-mode relaxation

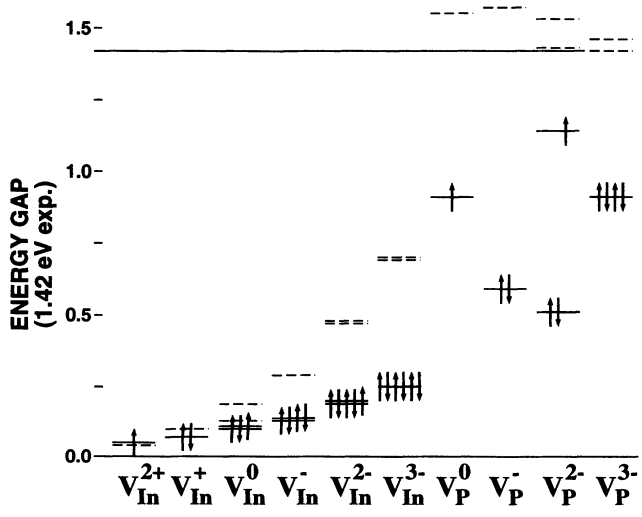

FIG. 1. The one-electron energy levels of the vacancies in InP. The dashed and the solid lines are the results of the unrelaxed and relaxed vacancies, respectively. The experimental width of the band gap is shown. All values are in eV.

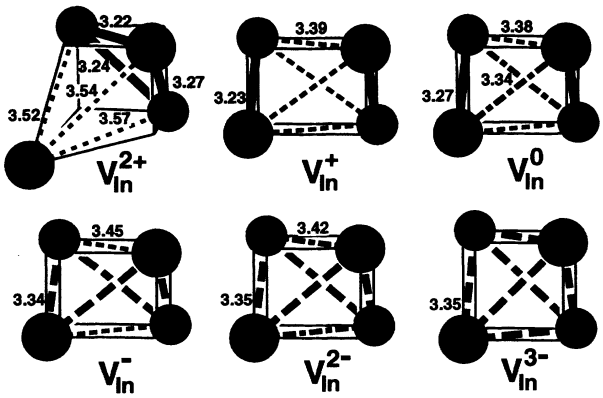

FIG. 2. The nearest-neighbor relaxations around In vacancies. The bond lengths are in Å.

for the indium vacancies is almost independent of the charge state. Fairly constant relaxations ensue from the relatively delocalized wave functions of the deep levels of the indium vacancies in all charge states. The breathing-mode amplitude ranges from -14.9% for V_{In}^{-} to -16.1% for V_{In}^{0} and the direction is thus inwards. The inward relaxation can be explained by the size of the In and P atoms: the small P atoms neighboring the In vacancy have plenty of space to relax towards the large open volume at the site of the missing In atom.

The pairing-mode relaxations in different charge states cannot be understood by simple space-filling arguments but by bonding properties of the electrons at the deep levels. For V_{In}^{3+} the T_2 deep levels would be empty and the T_d symmetry of the ideal vacancy would be conserved. When electrons are added to the triply degenerate T_2 level of the vacancy of T_d symmetry, the T_2 level splits and the symmetry is lowered (the Jahn-Teller theorem). Thus trigonal, tetragonal, and mixed distortions are expected for the charge states from V_{In}^{2+} to V_{In}^{2-}, as presented by Lannoo.[51]

In V_{In}^{2+} there is a single electron in the bound states in the gap. For V_{In}^{2+} the localized electron entering a previously unoccupied, degenerate state induces a trigonal distortion of symmetry C_{3v}: three of the nearest neighbors of the vacancy site form an equilateral triangle and the fourth neighbor is further away from the triangle.

TABLE II. The nearest-neighbor relaxation components for the different charge states of the indium vacancy in InP. A minus sign indicates a relaxation inward. Because of a trigonal relaxation mode, the breathing and pairing relaxation components are not well defined for V_{In}^{2+} and therefore not shown. The amplitudes are given in percent of the bulk bond distance of InP.

Vacancy	Breathing	Pairing 1	Pairing 2
V_{In}^{+}	-16.0	3.6	0.0
V_{In}^{0}	-16.1	2.0	0.7
V_{In}^{-}	-14.9	2.7	0.0
V_{In}^{2-}	-15.0	1.7	0.0
V_{In}^{3-}	-15.5	0.0	0.0

The relaxation amplitudes for V_{In}^{2+} are not listed in Table II because a trigonal distortion is not properly described by the directions of breathing and pairing components chosen for tetragonally distorted configurations.

The second band-gap electron of V_{In}^{+} is expected to occupy the same state as the previous electron. However, for V_{In}^{+} we find a very different configuration, where the two localized electrons form bonds between the nearest neighbors in a pairwise manner. Thus, the amplitude of the pairing-1 relaxation in Table II is nonzero (3.6%). The symmetry group is tetragonal D_{2d}.

In V_{In}^{0} the third electron cannot occupy the same state as the first electron pair, but occupies a higher state and starts to form a bond between two new atom pairs. The symmetry is lowered and the degeneracy of the previously unoccupied level is lifted in agreement with the Jahn-Teller theorem. While the higher state is only partially occupied, the bonds between the new atom pairs are weaker (and the bonds are longer) than those formed by the first electrons occupying the lower state in the gap. In Table II, the pairing-1 component is 2.0%, and the pairing-2 relaxation is 0.7%. The distorted vacancy has then an orthorhombic symmetry D_2.

In V_{In}^{-} the fourth electron occupies the same state as the third electron, and the bonds due to the electrons in the lower and higher states become equally strong. The amplitude of the pairing-1 mode is 2.7%, and the pairing-2 component is again zero. The symmetry group is D_{2d}.

The fifth electron in V_{In}^{2-} occupies a new state and starts to form a bond between the nearest neighbors that are furthest away from each other. The effect is so weak that the symmetry D_{2d} from V_{In}^{-} is preserved. The pairing-1 mode relaxation is 1.7% and the pairing-2 component is zero.

In V_{In}^{3-} the gap states are fully occupied by six electrons. The bond lengths between the nearest-neighbor atoms are equal and the vacancy has a tetrahedral symmetry T_d as for the unrelaxed vacancy. Both pairing-1 and pairing-2 components vanish.

The ionization levels of the vacancies (the values of the chemical potential at which the charge state changes[52]) are shown in Fig. 3. The ionization levels for the unrelaxed and relaxed vacancies from our CP simulations are shown in comparison with the results for the unrelaxed vacancies from Green's-function (GF) calculations.[28] For the indium vacancies all the ionization levels lie below midgap, in agreement with the GF results. Jansen[26] has also derived the ionization levels of the unrelaxed In vacancies using density-functional theory. Jansen found ionization levels for the transition $(2-/-)_{V_{In}}$ at 0.12 eV and for $(3-/2-)_{V_{In}}$ at 0.31 eV. These are quite close to our results for the unrelaxed In vacancies. However, the CP calculations predict that the relaxed In vacancy is positive when the Fermi level is close to the top of the valence-band maximum. This is consistent with preliminary results from positron-lifetime experiments, which do not indicate positron trapping to vacancies in p-type InP, i.e., the vacancies in the sample are positively charged when the Fermi level is close to the top of the valence-band maximum.[6]

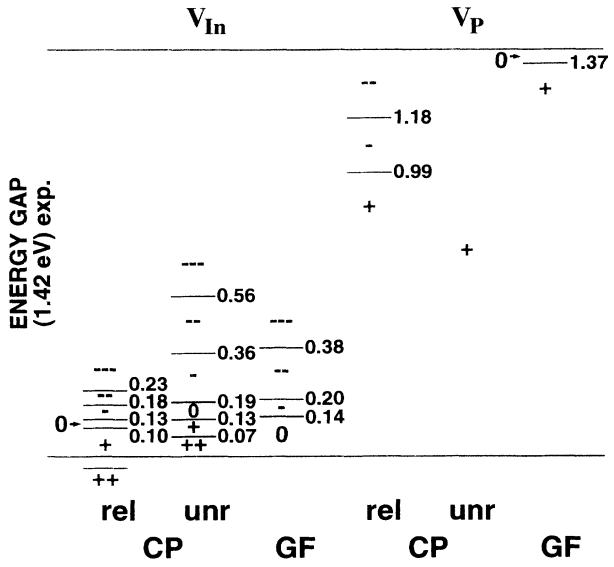

FIG. 3. The ionization levels for the unrelaxed and relaxed vacancies from our CP simulation, and for the unrelaxed vacancies from Green's-function (GF) calculations (Ref. 28). All values are given in eV relative to the top of the valence band.

Our results for In vacancies in InP show analogies with the CP results for Ga vacancies in GaAs.[32] Relaxations of Ga vacancies are almost independent of the charge state of the vacancy. The direction of the breathing-mode relaxation is always inwards and the pairing components are small. However, the amplitudes of the breathing-mode relaxations of Ga vacancies in GaAs are only a few percent, which is much smaller than those for In vacancies in InP. The one-electron energy eigenvalues for Ga vacancies in Ref. 32 were calculated slightly differently from our results for In vacancies in Fig. 1, but if they are analyzed using the same formalism, the positions of the eigenvalues relative to the top of the valence band agree within about one tenth of an eV.

B. Phosphorus vacancies

We have studied the phosphorus vacancies in charge states from singly positive V_P^{+} to triply negative V_P^{3-}, where the bound gap states are occupied by from zero to four electrons, respectively. The results for the phosphorus vacancies are slightly changed from those presented in Ref. 35 because the orthogonalization is now performed in a more consistent manner. The positive phosphorus vacancy V_P^{+}, was found to have been trapped to a flat, local-energy minimum, and when the calculation was continued the total energy relaxed to a lower value. The one-electron eigenvalues corresponding to the occupied gap states are shown in Fig. 1. For the unrelaxed P vacancies (dashed lines) the eigenvalues are above the experimental conduction-band minimum corresponding to continuum states. For the relaxed vacancies (solid lines) the eigenvalues are at the middle and upper parts of the gap. Thus when compared to In vacancies, the removal of one P atom with five valence electrons is a

more severe disturbance, pushing the defect-induced electron levels deeper in the gap.

Figure 4 is a schematic picture of the distortions of the lattice around the P vacancies in different charge states. The site of the missing P atom is at the center of the cube and the nearest-neighbor In atoms (filled circles) are at the corners. Table III shows the amplitudes of the nearest-neighbor relaxations as a percent of the bond distance of bulk InP. For P vacancies the charge state dependence of the relaxations is substantial. The breathing-mode amplitude increases monotonically from -5.5% for V_P^+ to -17.1% for V_P^{2-} with increasing electron density. The breathing-mode relaxation is smaller for the non-negative P vacancies than for the In vacancies, because the open space created by removing one P atom is smaller.

In V_P^+ there are no electrons in the gap states, and no symmetry-lowering relaxations occur. The distances between nearest-neighbor atoms are equal. The point-symmetry group of the structure is the tetrahedral T_d.

In V_P^0 there is a single electron at the defect-induced state, which causes a symmetry-lowering distortion according to the Jahn-Teller theorem. Bonds are formed between nearest neighbors in a pairwise manner, resulting in a pairing-1 relaxation of 9.0%. The symmetry of the configuration is D_{2d}.

The second electron of V_P^- occupies the same state as the first electron. This further strengthens the pairing-1 distortion to 15.3%. The symmetry D_{2d} is conserved.

In V_P^{2-} the third electron occupies an energy level higher in the gap. Large changes in the distortions are not observed: the pairing-1 component increases slightly to 17.0%, and the pairing-2 component is negligible. This is different from the distortions of the neutral In vacancy (with an equal number of electrons at the gap states), where the pairing-2 relaxation is nonzero. In V_P^{2-} the third electron has the same symmetry as the first and second, but the nodal surface structure of the highest state is more complicated (see Fig. 5). The symmetry for V_P^{2-} is still D_{2d}.

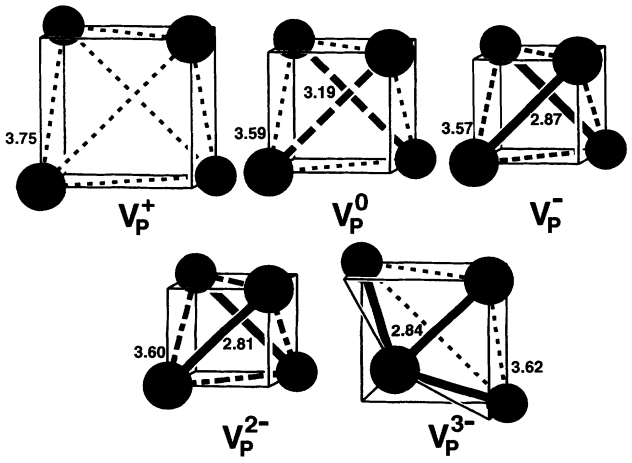

FIG. 4. The nearest-neighbor relaxations around P vacancies. The bond lengths are in Å

TABLE III. The nearest-neighbor relaxation components for the different charge states of the phosphorus vacancy in InP. A negative breathing-mode relaxation indicates a relaxation inward. Because of a trigonal relaxation mode, the breathing and pairing relaxation components are not well defined for V_P^{3-} and therefore now shown. The amplitudes are given in percent of the bulk bond distance of InP.

Vacancy	Breathing	Pairing 1	Pairing 2
V_P^+	−5.5	0.0	0.0
V_P^0	−13.2	9.0	0.0
V_P^-	−16.8	15.3	0.0
V_P^{2-}	−17.1	17.0	0.0

In V_P^{3-} the fourth electron causes trigonal distortion of symmetry C_{3v}. The amplitudes of the relaxations are not shown in Table III because the directions chosen for breathing and pairing modes are not well defined for trigonal symmetry.

The electron density of the highest occupied one-electron state is shown in Fig. 5. For V_P^{2-} the highest two states are shown separately. The highest electrons are very localized at the vacancy and form bonds between the nearest-neighbor atoms. The electron densities of the highest states of V_P^0 and V_P^-, and of the second-highest state of V_P^{2-}, show a clear pairwise bond formation between the nearest-neighbor indium atoms. The strength of the bond increases when going to more negative vacancies. The highest state of V_P^{2-} is more delocalized than the second highest because it is close to the conduction band (see Fig. 1). However, the highest state of F_P^{2-} is concentrated between the same atoms as the strongly

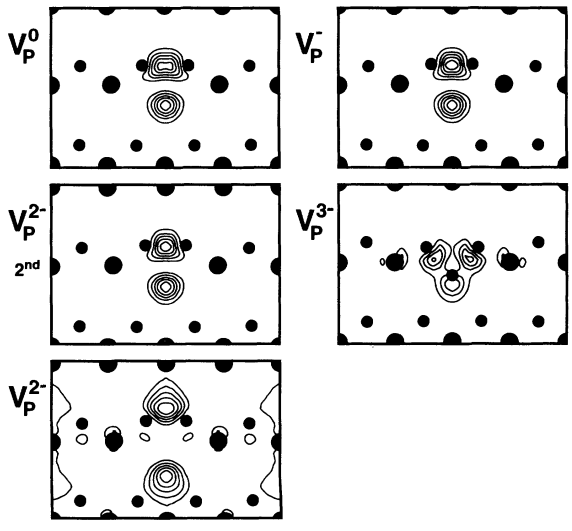

FIG. 5. The electron density of the highest occupied states of the phosphorus vacancies in different charge states. The highest two electron states are shown separately for V_P^{2-}. For V_P^{3-} the sum of the highest state densities is shown. The contour-level separation is one-sixth of the maximum value.

bonding second-highest electrons. Thus the third electron of V_P^{2-} is concentrated between the same atoms as the strongly bonding second-highest electrons. Thus the third electron of V_P^{2-} does not form a bond between two atom pairs as in V_{In}^0 but only further strengthens the relaxations already present in V_P^-.

The ionization levels for the relaxed phosphorus vacancies in Fig. 3 show the negative-U effect:[35] the charge state changes directly from V_P^+ to V_P^- when the electron chemical potential is raised in the gap. Thus the neutral P vacancy is not stable because of lattice relaxation. However, the increased computational accuracy does not confirm the direct transition from V_P^- to V_P^{3-} as reported in Ref. 35. Our results show that the P vacancy is negative when the Fermi level is in the upper part of the band gap. This is in agreement with the interpretation of the recent positron-lifetime experiments where positron trapping to P vacancies is seen in n-type InP but not in p-type samples.[6] In contrast, the charge state of the unrelaxed P vacancy is always positive, as also in other theoretical works,[23,26] or there is a $(0/x)_{V_P}$ ionization level just below the conduction band (the GF calculations in Fig. 3).[28] Therefore, for a proper description of the ionization levels of the P vacancies it is essential to consider fully relaxed vacancies.

Our results for the P vacancies in InP show the same behavior as the CP results for As vacancies in GaAs.[32] The inward-breathing mode and the pairing-1 components increase when the vacancy becomes more negative (in non-negative As vacancies there is a small outward relaxation that is not seen in P vacancies). In the singly and doubly negative P and As vacancies the amplitudes of the breathing and pairing modes are almost the same, about 17%. Also the highest-occupied electron state of V_{As}^- in Ref. 32 and V_P^- in Fig. 5 are very similar. When the one-electron energy eigenvalues of the As vacancies in Ref. 32 are calculated similarly to our results for InP, the eigenvalues of As vacancies in GaAs and P vacancies in InP are both close to the midgap. The eigenvalues of V_{As}^- and V_P^-, and the eigenvalues of V_{As}^{2-} and V_P^{2-} are similarly located, but the analogy is not so clear for the neutral vacancies.

C. Indium antisites

The indium antisites are studied from doubly positive In_P^{2+} to doubly negative In_P^{2-}. The occupation of the defect-induced states varies then from two to six, respectively. Figure 6 shows the corresponding one-electron eigenvalues relative to the top of the valence band. For In antisites the position of the one-electron eigenvalues rises in the gap as the number of electrons increases, which resembles the trend for In vacancies. However, for In antisites the levels are in the midgap and the level splittings can be large.

Figure 7 shows schematically the distortion of the In antisite and its four nearest-neighbor In atoms. The relaxation amplitudes are listed in Table IV. The breathing-mode relaxations around the In antisites are outward, because a smaller P atom is replaced by a larger In atom. The outward relaxation is largest for the positive antisites (11.3% for In_P^{2+}), in which the Coulomb repulsion between the positive In antisite with its nearest-neighbor cation atom cores is strongest.

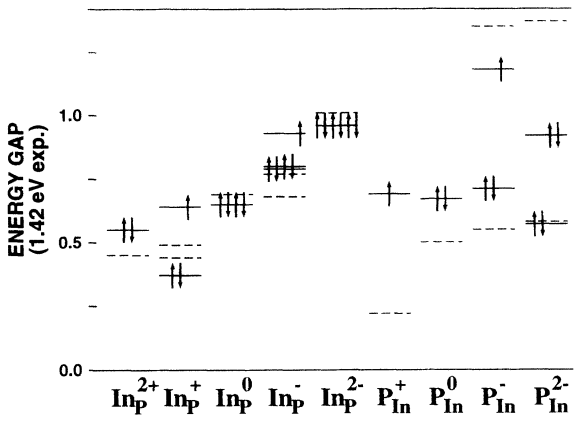

FIG. 6. The one-electron energy levels of the antisites in InP. The dashed and the solid lines are the results of the unrelaxed and relaxed antisites, respectively. The experimental width of the band gap is shown. All values are in eV.

Low-symmetry relaxations around the In antisites are found when the bound gap states are partially occupied. In In_P^{2+} the two bound gap electrons attract the nearest-neighbor atoms, giving rise to small pairing-1 and pairing-2 relaxations. The antisite atom is slightly shifted from the center of the cube. In In_P^+ the third electron occupies a new state and causes a nearly trigonal Jahn-Teller distortion: the antisite atom is shifted from the center of the cube to the center of the plane formed by three of its nearest neighbors. The symmetry of In_P^+ is close to trigonal with an additional tetragonal component. In In_P^0 with four bound gap electrons the relaxations are nearly tetragonal (D_{2d}) around the antisite that stays at the center. The tetragonal symmetry is reduced in In_P^- by the fifth electron, according to the Jahn-Teller theorem: the symmetry of In_P^- is a mixture of tetragonal and trigonal modes. The relaxation amplitudes are, however, very small. Finally, the T_2 level of In_P^{2-} is fully occupied with the tetrahedral symmetry of the ideal

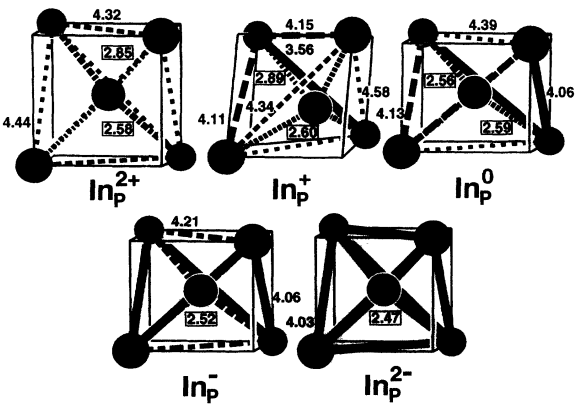

FIG. 7. The nearest-neighbor relaxations around In antisites. The bond lengths are in Å.

TABLE IV. The nearest-neighbor relaxation components for the different charge states of the indium antisite in InP. A positive breathing-mode relaxation indicates a relaxation outward. Because of a trigonal relaxation mode, the breathing and pairing relaxation components are not well defined for In_P^+ and therefore not shown. The amplitudes are given in percent of the bulk bond distance of InP.

Antisite	Breathing	Pairing 1	Pairing 2
In_P^{2+}	11.3	3.7	−1.7
In_P^0	5.5	3.6	−6.2
In_P^-	3.5	1.8	−3.2
In_P^{2-}	1.5	0.0	0.0

antisite. The pure breathing-mode relaxation of In_P^{2-} is outward with an amplitude of only 1.5%.

The ionization levels for indium antisites from our CP simulations are shown in Fig. 8, together with the GF results for the unrelaxed defects.[28] The ionization levels for the unrelaxed antisites are at midgap and in the lower half of the gap. The levels from GF calculations are little lower than those from CP calculations. After relaxation, a negative-U effect is observed from In_P^{2+} to In_P^0. Relaxation also shifts the position of the ionization levels to the midgap so that $(0/2+)_{In_P}$ lies at 0.68 eV, $(-/0)_{In_P}$ at 0.91 eV, and $(2-/-)_{In_P}$ at 0.95 eV above the valence-band maximum.

In the *ab initio* LDA calculations for the cation antisites in GaAs by Zhang and Chadi,[53] a direct transformation from the neutral Ga_{As}^0 to the doubly negative Ga_{As}^{2-} state is observed. However, the relaxations of Ga_{As}^0 are large and clearly different from our result for In_P^0.

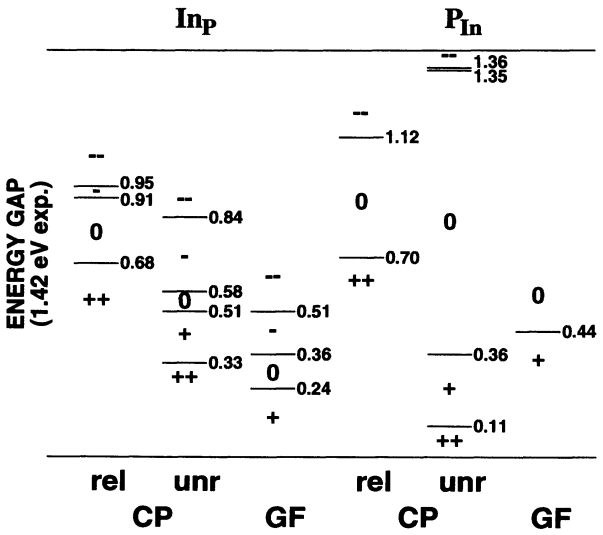

FIG. 8. The ionization levels for the unrelaxed and relaxed antisite defects from our CP simulation, and for the unrelaxed antisites from Green's-function (GF) calculations (Ref. 28). All values are given in eV relative to the top of the valence band.

D. Phosphorus antisites

The phosphorus antisites are studied from doubly positive P_{In}^{2+} to doubly negative P_{In}^{2-}. The anion antisite induces three localized states, of which two are electrically inactive (low in energy and fully occupied) and the third lies in the fundamental energy gap. Figure 6 shows the calculated positions and the occupancy of the corresponding one-electron eigenvalues for P antisites. The level positions for the relaxed P antisites are at midgap or above. In P_{In}^{2+} the defect-induced A_1 state in the gap is empty. In P_{In}^+ and P_{In}^0 the A_1 gap state is occupied by one and two electrons, respectively, and in P_{In}^- and P_{In}^{2-} also the state arising from the T_2 level of the unrelaxed antisite has one and two electrons, respectively. For the tetrahedral P_{In}^0 antisite, the one-electron eigenvalue corresponding to the A_1 state is at ~0.7 eV above the valence-band maximum (0.5 eV for the unrelaxed P_{In}^0), which is in very good agreement with the corresponding value of 0.68 eV (0.57 eV for the unrelaxed P_{In}^0) derived from the first-principles supercell calculations by Caldas *et al.*[27]

The position of the one-electron energy levels for the anion antisites in GaAs has recently been studied by Ziegler *et al.*[54] using the GF method and scissors operator. They recalculated the 54-atom supercell results by Dabrowski and Schefler[34] for the As atom in GaAs displaced from the antisite position As_{Ga} to the interstitial position $V_{Ga}As_i$. They found that the wave functions and the positions of the one-electron energy levels in the stable As_{Ga} and metastable $V_{Ga}As_i$ geometries from the GF calculations were practically the same as those from the supercell calculations. However, noticeable differences were found when the As atom was displaced from the stable or metastable state. Similarly, in our calculation for InP the effect of the supercell approximation (with 64 atoms) should be smallest when the one-electron energies for the ground-state structure are studied.

Figure 9 shows schematically the distortion of the nearest-neighbor P atoms around the phosphorus antisites. The relaxation amplitudes are listed in Table V. The breathing-mode relaxations around the P antisites

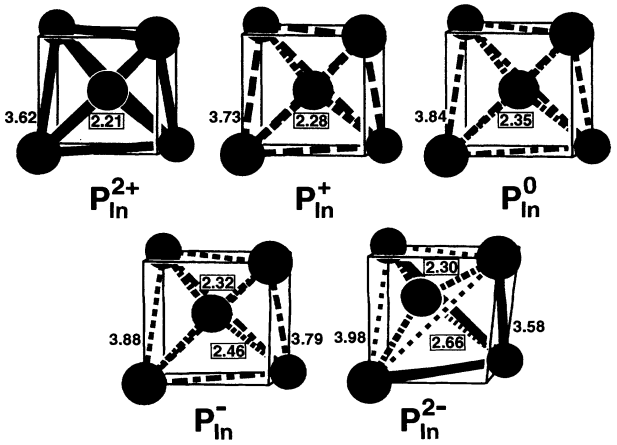

FIG. 9. The nearest-neighbor relaxations around P antisites. The bond lengths are in Å.

TABLE V. The nearest-neighbor relaxation components for the different charge states of the phosphorus antisite in InP. A negative breathing-mode relaxation indicates a relaxation inward. Because of a trigonal relaxation mode, the breathing and pairing relaxation components are not well defined for P_{In}^{-} and P_{In}^{2-} and therefore not shown. The amplitudes are given in percent of the bulk bond distance of InP.

Antisite	Breathing	Pairing 1	Pairing 2
P_{In}^{2+}	−8.8	0.0	0.0
P_{In}^{+}	−6.0	0.0	0.0
P_{In}^{0}	−3.3	0.0	0.0

are always inward, because a larger In atom is replaced with a smaller P atom. The inward relaxation is largest for the most positive antisite (-8.8% for P_{In}^{2+}) in which the Coulomb attraction between the antisite and its nearest-neighbor anion atom cores is strongest. According to the *ab initio* calculations by Caldas *et al.*[27] for the neutral anion antisites the inward relaxation is exceptional in the case of the P antisite in comparison with the larger anion substitutes (As,Sb) in InP.

Since in the doubly positive, singly positive, and neutral P antisites all bound states in the gap are unoccupied or only the A_1 bound states are occupied, no Jahn-Teller relaxations are observed. The tetrahedral symmetry T_d of the ideal vacancy is preserved. In P_{In}^{-} one electron occupies the state formed from the T_2 level of the unrelaxed defect, causing a trigonal distortion due to the Jahn-Teller effect. Because of the antibonding character of the highest-energy wave function the bond between the P_{In}^{-} antisite atom and one of its nearest-neighbor atoms is weakened. The antisite atom is slightly shifted towards the plane formed by three of the nearest-neighbor atoms that form an equilateral triangle. The trigonal distortion is further strengthened in P_{In}^{2-}, where the second electron enters the same state that is already occupied in P_{In}^{-}. The antisite atom has moved further toward the plane of the three equally separated nearest neighbors. The trigonal relaxation modes for P_{In}^{-} and P_{In}^{2-} show analogies with the bonding mechanism proposed for the *EL*2 and *DX* defects in GaAs.[34,55]

Figure 8 shows the ionization levels for phosphorus antisites from our CP simulations and from the GF calculations.[28] Only the $(0/+)_{P_{In}}$ level at 0.44 eV for the unrelaxed antisites has been calculated within the GF method.[28] This is in agreement with the CP result of$(0/+)_{P_{In}}$ at 0.36 eV for the unrelaxed phosphorus antisites. The CP calculations show that relaxation changes substantially the position of the ionization levels of P antisites. After relaxation, both the doubly positive and the neutral states of the P antisite capture two electrons rather than one, resulting in two, yet very narrow, negative-U effects, $(0/2+)_{P_{In}}$ at 0.7 eV and $(2-/0)_{In_P}$ at 1.1 eV above the valence-band maximum. However, the *ab initio* simulations of Caldas *et al.*[27] give a single ionization level $(0/+)_{P_{In}}$ at 0.95 eV (at 0.78 for the unrelaxed defects), which is calculated using two special **k** points to reduce the finite-size effects of the 54-atom supercell. These results are in contrast to our values.

The ODENDOR experiments on *p*-type InP propose a tetrahedral symmetry for the P antisites.[13,14] This is not in contrast to our results, which predict that the tetrahedral doubly positive antisite P_{In}^{2+} is the dominating P antisite when the electron chemical potential is in the lower part of the band gap. In Ref. 14 the authors have found the wave function in P_{In}^{+} to be highly localized, in good agreement with our results, where the singly positive and the neutral P antisites have a well-localized A_1 highest state. Also the wave functions for our singly and doubly negative antisites form a localized highest state, which this time has a trigonal symmetry and a nodal plane between the antisite atom and the single, next-nearest-neighbor atom. Thus it is an antibonding state. We have verified that the gap states belong to the A_1 presentation of the C_{3v} symmetry group. Our results are in qualitative agreement with the energy level structure for the slightly displaced As antisite atom in GaAs.[34,55] However, this is the first time that negative phosphorus antisites have been reported in the literature to our knowledge.

The experimental estimate for the $(+/2+)_{P_{in}}$ ionization level is at about 1 eV above the valence-band edge[15,16] which cannot be confirmed by our calculations. However, a comparison with the ionization-level positions in low-temperature molecular-beam-epitaxy-grown InP_{15} may be meaningless because of the high concentration of defects in the sample.

E. Defect formation energies

The formation energies predict the thermodynamically preferred defects in the material. The formation energy depends on the electron chemical potential (position of the Fermi level in the gap) and on the atomic chemical potentials. In compound semiconductors the ratio of the constituent species (stoichiometry) also has to be taken into account.[56] Experimentally, the ratio of the constituent species, i.e., the atomic chemical potentials, can be controlled by annealing the system under either anion- or cation-rich conditions. Following Zhang and Northrup[57] we have calculated the vacancy formation energies as a function of the electron chemical potential μ_e and the parameter $\Delta\mu$. $\Delta\mu$ is defined as

$$\Delta\mu=(\mu_C-\mu_A)-(\mu_{c,\text{bulk}}-\mu_{A,\text{bulk}}) , \quad (1)$$

where μ_C and μ_A are the cation and anion chemical potentials in the compound, and $\mu_{C,\text{bulk}}$ ($\mu_{A,\text{bulk}}$) is the chemical potential of the cation (anion) atoms in a bulk material consisting of only cations (anions). The formation energy Ω of the defect in charge state Q is then

$$\Omega=E_Q^*[N_A,N_C]+Q(E_v+\mu_e)-\tfrac{1}{2}(N_C-N_A)\Delta\mu , \quad (2)$$

where μ_e is the chemical potential relative to the top of the valence band E_v, and N_A and N_C are the number of anion and cation atoms, respectively. $E_Q^*[N_A,N_C]$ is defined as

$$E_Q^*[N_A,N_C]=E_Q[N_A,N_C]-\tfrac{1}{2}(N_C+N_A)\mu_{A+C} -\tfrac{1}{2}(N_C-N_A)(\mu_{C,\text{bulk}}-\mu_{A,\text{bulk}}) , \quad (3)$$

where $E_Q[N_A,N_C]$ is the total energy of the supercell with a defect and $\mu_{A+C}=\mu_A+\mu_C$ is the chemical potential of an anion-cation "dimer" in the compound.

In InP the electron chemical potential μ_e can have values between 0 and 1.42 eV, corresponding to the experimental band-gap width. The parameter $\Delta\mu$ is tuned from $-\Delta H$ to ΔH, where ΔH is the heat of formation of InP.[57] Using cohesion energies calculated for bulk In and P, we have determined that the heat of formation $\Delta H=0.94$ eV. This is close to the experimental value of 0.92 eV.[58] In Fig. 10 we show the formation energies (in the preferred charge states) for the vacancies and antisites as a function of $\Delta\mu$. Only the ground-state configurations are shown. The formation energies are calculated from Eq. 2 at three values of the electron chemical potential: at the valence-band maximum (VBM), at midgap ($E_g/2$), and at the conduction-band minimum (CBM). When going towards more negative (positive) values of $\Delta\mu$, from Eq. 1 the P (In) concentration increases. Although the formation energies are shown in the range of allowed values of $\Delta\mu$ and ΔH, the extreme values for $\Delta\mu$ and ΔH may not be obtained simultaneously. The formation energies of the P vacancy and the P antisite are lower than those of the In vacancy and In antisite for all values of $\Delta\mu$ when the electron chemical potential is at the midgap or below. Therefore P vacancies and P antisites should be seen in p-type and semi-insulating samples. If the electron chemical potential is close to the maximum of the valence band, the P antisites and vacancies should be positive. If the electron chemical potential is in the upper part of the gap, both V_{In}^{3-} and V_P^{2-} should be observed. The concentration of P vacancies (P antisites) in P-rich material is, of course, smaller (larger) than in In-rich material. To be able to predict the actual concentrations of defects, however, a thorough calculation (with interstitials, defect complexes, and dopants included) should be carried out.[56]

The defect formation energies for defects in InP resemble the results for defects in GaAs obtained by Zhang and Northrup.[57] Anion antisites (As_{Ga} in GaAs and P_{In} in InP) are observed in anion-rich material when the Fermi-level is at midgap or below. Cation vacancies (V_{Ga} in GaAs and V_{In} in InP) should be seen in anion-rich compounds if the Fermi level is close to the conduction-band minimum. However, the Ga antisite is the prevalent defect in cation-rich GaAs when the Fermi level is at midgap or above. In InP we do not expect to find cation antisites (In_P) at equilibrium, which is in accordance with the fact that no experimental results, to our knowledge, have been attributed to In_P.

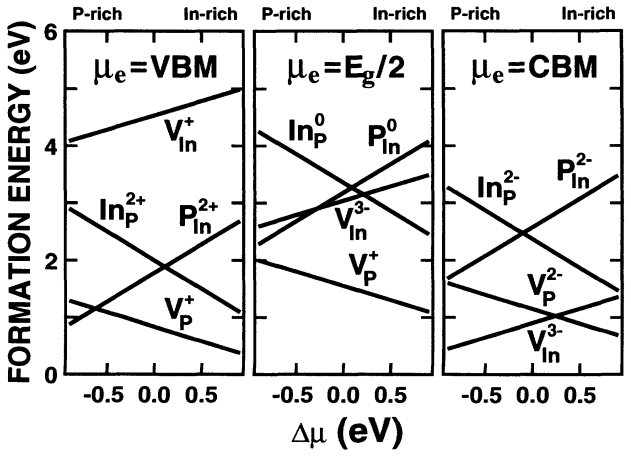

FIG. 10. The formation energies for the vacancies and antisites in indium phosphide at three values of the Fermi-level position: at the top of the valence band (VBM), at midgap ($E_g/2$), and at the bottom of the conduction band (CBM).

IV. SUMMARY

The relaxation patterns around vacancies and antisites in InP arise from the size and charge of the atoms in the defect complex and from the bonding properties of the electrons in the bound states. The distortions near the defects have tetrahedral, trigonal, tetragonal, or mixed trigonal-plus-tetragonal symmetry. The competition between the bond formation and the free space for the ions introduces breathing-mode relaxations that do not lower the symmetry of the ideal tetrahedral defect. The symmetry-lowering relaxations occur when an orbitally degenerate level is partially occupied by electrons, whose effect is to split the level and thus lower the energy. Which symmetry is favored, tetragonal or trigonal, depends upon the defect considered and is difficult to predict, as discussed by Lannoo.[51]

The relaxations around the defects can be understood in terms of hybridization for the s and p valence electrons of the In and P atoms. Trigonal distortions, such as the relaxations of the negative P antisites, arise from sp^2 hybridized bonds between the antisite and its nearest neighbors. In the tetragonal geometries, sp^3 hybridization takes place. The variety of different configurations is a general property of sp-bonded materials and it is expected to be responsible for the metastable defects (DX and $EL2$) in III-V compounds.[59]

In conclusion, using the first-principles Car-Parrinello method we have performed symmetry-unrestricted optimizations of the valence-electron structure and ionic positions of the vacancies and antisites in InP. Large tetrahedral, trigonal, and tetragonal lattice relaxations are found, indicating strong interplay between the electronic structure and atomic positions. In general, the effect of distortions changes the qualitative picture derived for unrelaxed defects, and thus cannot be omitted. Relaxation gives rise to negative-U phenomena, which are expected to be a common property in compound semiconductors. We find that in phosphorus-rich material In vacancies (n type) and P antisites (p type) should dominate, while in indium-rich material the prevalent defect should be the P vacancy.

ACKNOWLEDGMENTS

This research has been supported in part by Academy of Finland. We are also grateful to Centre for Scientific Computing, Espoo, Finland, for generous supercomputing resources and to Dr. Kari Laasonen for many fruitful discussions.

[1]O. Oda, K. Katagiri, S. Shinohara, S. Katsura, Y. Takahashi, K. Kainosho, K. Kohiro, and R. Hirano, *InP Crystal Growth, Substrate Preparation and Evaluation,* Vol. 31 of *Semiconductors and Semimetals* (Academic, New York, 1990), p. 93.

[2]M. Deiri, A. Kana-ah, B. C. Cavenett, T. A. Kennedy, and N. D. Wilsey, Semicond. Sci. Technol. **3**, 706 (1988).

[3]J. Frandom, F. Fabre, G. Bacquet, J. Bandet, and F. Reynaud, J. Appl. Phys. **59**, 1627 (1986).

[4]H. Temkin, B. V. Dutt, and W. A. Bonner, Appl. Phys. Lett. **38**, 431 (1981).

[5]S. Palko, M. S. thesis, Helsinki University of Technology, 1992.

[6]K. Saarinen (private communication).

[7]H. J. von Bardeleben, Solid State Commun. **57**, 137 (1986).

[8]M. Yamada, P. K. Tien, R. J. Martin, R. E. Nahory, and A. A. Ballman, Appl. Phys. Lett. **43**, 594 (1983).

[9]B. Tuck and A. Hooper, J. Phys. D **8**, 1806 (1975).

[10]G. Dlubec, O. Brümmer, F. Plazaola, P. Hautojärvi, and K. Naukkarinen, Appl. Phys. Lett. **46**, 1136 (1985).

[11]T. A. Kennedy and N. D. Wilsey, Appl. Phys. Lett. **44**, 1089 (1984).

[12]A. Kana-ah, M. Deiri, B. C. Cavenett, N. D. Wilsey, and T. A. Kennedy, J. Phys. C **18**, L619 (1985).

[13]H. C. Crookham, T. A. Kennedy, and D. J. Treacy, Phys. Rev. B **46**, 1377 (1992).

[14]D. Y. Jeon, H. P. Gleason, J. F. Donegan, and G. D. Watkins, Phys. Rev. B **36**, 1324 (1987).

[15]P. Dreszer, W. M. Chen, K. Seendripu, J. A. Wolk, W. Walukiewicz, B. W. Liang, C. W. Tu, and E. R. Weber, Phys. Rev. B **47**, 4111 (1993).

[16]H. P. Gislason, H. Sun, R. E. Peale, and G. D. Watkins, Mater. Sci. Forum **83-87**, 905 (1992).

[17]M. Levinson, J. L. Benton, and L. C. Kimerling, Phys. Rev. B **27**, 6216 (1983); M. Levinson, M. Stavola, J. L. Benton, and L. C. Kimerling, Phys. Rev. B **28**, 5848 (1983); M. Stavola, M. Levinson, J. L. Benton, and L. C. Kimerling, Phys. Rev. B **30**, 832 (1984).

[18]J. F. Wager and J. A. van Vechten, Phys. Rev. B **32**, 5251 (1985).

[19]M. Levinson, M. Stavola, P. Besomi, and W. A. Bonner, Phys. Rev. B **30**, 5817 (1984).

[20]Z.-Q. Fang, D. C. Look, and J. H. Zhao, Appl. Phys. Lett. **61**, 589 (1992).

[21]J. A. Wolk, W. Walukiewicz, M. L. W. Thewalt, and E. E. Haller, Phys. Rev. Lett. **68**, 589 (1992).

[22]D. J. Chadi and K. J. Chang, Phys. Rev. Lett. **61**, 873 (1988); D. J. Chadi and K. J. Chang, Phys. Rev. B **39**, 10 063 (1989).

[23]Hongqi Xu, Phys. Rev. B **42**, 11 295 (1990).

[24]P. J. Lin-Chung and T. L. Reinecke, Phys. Rev. B **27**, 1101 (1983).

[25]D. N. Talwar and C. S. Ting, Phys. Rev. B **25**, 2660 (1982).

[26]Robert W. Jansen, Phys. Rev. B **41**, 7666 (1990).

[27]M. J. Caldas, J. Dabrowski, A. Fazzio, and M. Scheffler, Phys. Rev. Lett. **65**, 2046 (1990).

[28]M. J. Puska, J. Phys. Condens Matter **1**, 7347 (1989).

[29]T. Bretagnon, G. Bastide, and M. Routzeyere, Phys. Rev. B **40**, 3749 (1989).

[30]R. Car and M. Parrinello, Phys. Rev. Lett. **55**, 2471 (1985); I. Štich, R. Car, and M. Parrinello, Phys. Rev. B **44**, 4262 (1991).

[31]R. Virkkunen, M. Alatalo, M. J. Puska, and R. M. Nieminen, Comput. Mater. Sci. **1**, 151 (1993).

[32]K. Laasonen, R. M. Nieminen, and M. J. Puska, Phys. Rev. B **45**, 4122 (1992).

[33]Q.-M. Zhang and J. Bernholc, Phys. Rev. B **47**, 1667 (1993).

[34]Jaroslaw Dabrowski and Matthias Scheffler, Phys. Rev. B **40**, 10 391 (1989).

[35]M. Alatalo, R. M. Nieminen, M. J. Puska, A. P. Seitsonen, and R. Virkkunen, Phys. Rev. B **47**, (1993).

[36]See, e.g., R. O. Jones and O. Gunnarsson, Rev. Mod. Phys. **61**, 689 (1989).

[37]G. Pastore, E. Smargiassi, and F. Buda, Phys. Rev. A **44**, 6334 (1991).

[38]R. Stumpf, X. Gonze, and M. Scheffler (unpublished).

[39]G. B. Bachelet, D. R. Hamann, and M. Schlüter, Phys. Rev. B **26**, 4199 (1982).

[40]L. Kleinman and D. M. Bylander, Phys. Rev. Lett. **48**, 1425 (1982).

[41]B. Delley, J. Chem. Phys. **92**, 508 (1990).

[42]*Semiconductors: Group IV Elements and III-V Compounds,* edited by O. Madelung, Data in Science and Technology Vol. 1 (Springer-Verlag, Berlin, 1991).

[43]J. Furthermüller and M. Fähnle, Phys. Rev. B **46**, 3839 (1992).

[44]William H. Press, Brian P. Flannery, Saul A. Teukolsky, and William T. Veterling, *Numerical Recipes* (Cambridge University Press, Cambridge, 1986).

[45]S. Kirkpatrick, C. D. Gelatt, Jr., and M. P. Vecchi, Science **220**, 671 (1983).

[46]M. L. Cohen, and J. R. Chelikowsky, in *Electronic Structure and Optical Properties of Semiconductors,* edited by M. Cardona, *Solid-State Sciences* Vol. 75 (Springer-Verlag, Berlin, 1988).

[47]S. Massidda, A. Continenza, A. J. Freeman, T. M. de Pascale, F. Meloni, and M. Serra, Phys. Rev. B **41**, 12 079 (1990).

[48]L. Ley, R. A. Pollak, R. R. McFeely, S. P. Kowalczyk, and D. A. Shirley, Phys. Rev. B **9**, 600 (1974).

[49]H. Mathieu, Y. Chen, J. Camassel, J. Allegre, and D. S. Robertson, Phys. Rev. B **32**, 4042 (1985).

[50]G. B. Bachelet and N. E. Christensen, Phys. Rev. B **31**, 879 (1985).

[51]M. Lannoo, Physica B **116**, 63 (1983).

[52]R. W. Jansen and O. F. Sankey, Phys. Rev. B **39**, 3192 (1989).

[53]S. B. Zhang and D. J. Chadi, Phys. Rev. Lett. **64**, 1789 (1990).

[54]Christine Ziegler, Udo Scherz, and Matthias Scheffler, Phys. Rev. B **47**, 16 624 (1993).

[55]Mineo Saito, Atsushi Oshiyama, and Osamu Sugino, Phys. Rev. B **45**, 13 745 (1992).

[56]For a thorough discussion of the effects of stoichiometry, atomic chemical potentials, and defect thermodynamics, see, e.g., H. Wenzl, W. A. Oates, and K. Mika, in *Handbook of Crystal Growth,* edited by D. T. J. Hurle (in press).

[57]S. B. Zhang and J. E. Northrup, Phys. Rev. Lett. **67**, 2339 (1991).

[58]*Handbook of Chemistry and Physics,* 67th ed., edited by R. C. Weast (CRC Press, Boca Raton, Florida, 1986).

[59]J. Dabrowski and M. Scheffler, Mater. Sci. Forum **83-87**, 735 (1992).